Shape Dynamics and Rheology of Soft Elastic Particles in a Shear Flow

Tong Gao, Howard H. Hu, and Pedro Ponte Castañeda

Phys. Rev. Lett. **108**, 058302 — Published 31 January 2012

DOI: 10.1103/PhysRevLett.108.058302

Shape Dynamics and Rheology of Soft Elastic Particles in a Shear Flow

Tong Gao[1], Howard H. Hu[1]* and Pedro Ponte Castañeda[1,2]
[1] *Department of Mechanical Engineering and Applied Mechanics, University of Pennsylvania, Philadelphia, PA 19104, USA*
[2] *IMDEA Materials Institute, Madrid, E-28040, Spain*

The shape dynamics of soft, elastic particles in an unbounded simple shear flow is investigated theoretically under Stokes flow conditions. Three types of motion—steady-state, trembling and tumbling—are predicted, depending on the shear rate, elastic shear modulus and initial particle shape. The steady-state motion is found to be always stable. In addition, the existence of a trembling regime is documented for the first time in non-vesicle systems, and a complete phase diagram is developed. The rheological properties of dilute suspensions of such soft particles generally exhibit shear-thinning behavior, and can even display negative intrinsic viscosity for sufficiently soft particles.

PACS numbers: 47.57.E-, 47.61.Jd, 83.10.Pp, 47.57.Qk

Microscale soft particles are commonly found in nature and engineering applications. Examples include red blood cells [1], fluid vesicles [2] and microgel particles [3]. When placed in a viscous flow, these particles can readily undergo large deformations to accommodate the hydrodynamic forces exerted by the fluid, and in turn have a significant impact on the macroscopic rheological properties of the fluid-solid mixture.

Because of the thin membranes, or shell-like structures surrounding them, biological cells and vesicles exhibit highly complex responses in fluid flows. Thus, it has been recognized that the membrane-area incompressibility in vesicles can lead to a rich class of morphologies under shear flow conditions [4–10]. However, other particle types, such as microgel particles and swollen starch granules, do not possess surrounding thin membranes, and have to be modeled differently. For example, it is known that initially spherical elastic particles admit steady-state (SS) solutions [11–13] characterized by the balance between the viscous force in the fluid and the elastic force in solid. In addition, compared to thin membranes, such "thick" elastic particles may be expected to be less susceptible to instabilities induced by ambient flows, leading to potentially very different dynamical behaviors.

Compared to the extensive efforts that have been devoted to understand the response of cells and vesicles in viscous flows, much less attention has been drawn to elastic particles, and a complete understanding of the effect of elastic particles in fluid flows is still lacking. One key challenge in the elastic particle systems is the difficulty in handling the inherently nonlinear hydrodynamic interactions between the fluid and the solid, particularly in the large-deformation regime [14]. Recently, we have established [15] a large-deformation theory for the response of an elastic particle in an unbounded Newtonian fluid subjected to a homogeneous remote field, by demonstrating (see also [12]) that the physical fields (stress, strain-rate, etc.) inside an initially ellipsoidal elastic particle are uniform, and making use of the well-known fact that an ellipsoidal elastic particle subjected to a linear deformation field (e.g., simple shear) will deform through a series of ellipsoidal shapes [11–13], with evolving size, shape and orientation. In this sense, the problem is similar to the classical Eshelby problem in the theory of composite materials [16], and was thus solved by means of a polarization technique originally developed for elasticity [17, 18].

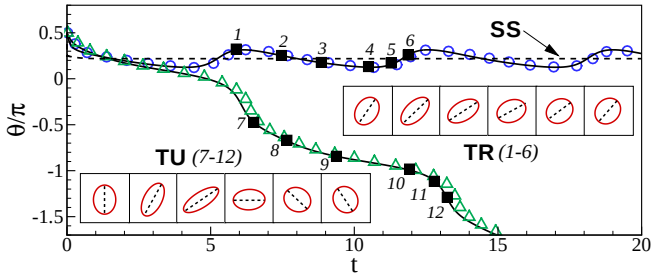

FIG. 1: Three types of particle motion under shear at $G = 0.2$. The solid black lines represent the unsteady TR and TU motions for initially elliptical (2D) particles, which are computed at $\omega_0 = 0.8$ and $\omega_0 = 0.6$, respectively. The dashed black line represent the SS motion of an initially circular ($\omega_0 = 1$) particle [11, 15]. The blue and green symbols are ALE FEM results (with $Re = 0.01$). Shape contours are shown sequentially at times indicated by black squares. The black dotted line is the particle's major axis.

In this Letter, we report on an analytical study of the dynamics of elastic particles undergoing arbitrarily large deformation in a simple shear flow. In contrast to prior studies [11, 12, 15, 19], which assumed that the initial shape of the elastic particles was perfectly symmetric (i.e., spherical, or circular in 2D models), in this work the particles are taken to have a non-trivial initial (spheroidal or elliptical) shape. This more general assumption is shown to give rise to a new type of motion for the particle—which is different from the steady-

*Electronic address: hhu@seas.upenn.edu

state (SS) motion observed for initially spherical particles [11, 12, 15, 19], and also different from the tumbling (TU) motion for rigid ellipsoidal particles [20]—but somewhat reminiscent of a certain type of trembling (TR) motion first observed in vesicles under shear flow conditions [5–10]. In addition, the conditions determining the TR/TU transition are identified, and the corresponding critical behaviors of shape change near the transition are elucidated. Finally, the rheological properties of dilute suspensions of the elastic particles—corresponding to the three types of motions—are characterized.

We consider an initially ellipsoidal (elliptical) particle immersed in an unbounded simple shear flow $\mathbf{U} = (\dot{\gamma}\bar{x}_2, 0, 0)$, where $\dot{\gamma}$ is the shear rate, and $\{\bar{x}_i\}$ is the fixed laboratory coordinate system. The particle is assumed to be a homogeneous, incompressible, neo-Hookean elastic solid with shear modulus S, while the surrounding fluid is Newtonian with viscosity η. It is then natural to define the dimensionless parameter, $G = \frac{\eta\dot{\gamma}}{S}$, representing the ratio of the viscous forces in the fluid to the elastic forces in the solid. When the particle undergoes a planar motion in the shear plane (e.g., the $\bar{x}_1 - \bar{x}_2$ plane), the evolution of the system can be described by a set of coupled, nonlinear, first-order ODEs in a rotating coordinate system $\{x_i\}$ aligned with the particle's axes for the aspect ratios of the particle, the orientation angle θ (defined from the horizontal axis to the long axis of the particle), and the "extra" stress $\boldsymbol{\tau}^p$ in the particle (total minus hydrostatic), as described in [21]. For an elastic particle with initially prolate spheroidal (or elliptical) shape, the initial conditions are provided by the initial aspect ratio ω_0, which will be taken to be between 0 and 1, the initial orientation θ_0, which produces only a time shift in the results and will therefore be fixed to take the value $\frac{\pi}{2}$, and $\boldsymbol{\tau}_0^p = \mathbf{0}$.

For simplicity, we begin with the 2D model problem involving a cylindrical particle with elliptical cross-section. As illustrated in Fig. 1 for a particle with a fixed value of G and different values of ω_0, three types of motion can be identified depending on the time evolution of θ. An initially circular particle ($\omega_0 = 1$) becomes elongated and rotates until reaching a stable configuration with a fixed orientation [15]. We emphasize, however, that although the particle shape reaches a SS, material elements inside the particle undergo a (periodic) tank-treading (TT) motion. For a slightly elongated particle ($\omega_0 = 0.8$), its long axis oscillates periodically in a TR motion, never making a full 2π rotation. As the initial shape becomes more elongated ($\omega_0 = 0.6$), the particle switches to a TU motion, with the long axis now making complete 2π rotations. Comparisons are also shown with direct numerical simulations (open circles) using an Arbitrary Lagrangian-Eulerian finite element method (ALE FEM) [19].

For the initially circular particle ($\omega_0 = 1$), the governing equations in 2D can be simplified to two equations for θ and ω [21], with steady-state solutions given by: $\omega = \left(\sqrt{1+G^2} - G\right)^2$, $\theta = \frac{1}{2}\arctan\left(\frac{1}{G}\right)$, $\tau_{11}^p = -\left(\tau_{22}^p\right)^{-1} = 2\left(\sqrt{1+G^2} + G\right)$, $\tau_{12}^p = 0$. A linear stability analysis

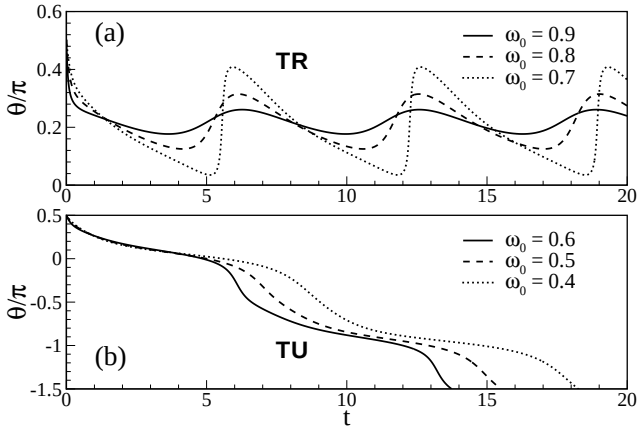

FIG. 2: Typical time-dependent solutions for θ at $G = 0.2$ in the (a) TR and (b) TU regimes.

leads to the two eigenvalues, $\lambda_\pm = -\frac{1+G^2}{(1+2G^2)G} \pm \frac{\sqrt{1+G^2}}{1+2G^2}i$ with strictly negative real parts, indicating that the SS motion is always stable, even for large particle deformation.

For fixed $G > 0$, as soon as the initial particle shape ceases to be circular ($\omega_0 < 1$), the particle motion becomes TR, and eventually switches to TU for sufficiently elongated particles ($\omega_0 \leq \omega_0^*$). Thus, as shown in Fig. 2(a), the amplitude of the oscillations in θ gradually increase (from 0) as ω_0 decreases (from 1), and at the same time, the transition from the minimum to maximum values becomes sharper, leading to a discontinuity at $\omega_0 = \omega_0^*$, beyond which the motion shifts into the TU regime. As shown in Fig. 2(b), θ undergoes complete rotations in the TU regime, with a time period that gradually increases as ω_0 continues to decrease below ω_0^*.

In the TR regime, we can carry out a perturbation analysis for nearly circular ($\omega_0 = 1 - \varepsilon, \varepsilon \ll 1$) particles; i.e., $\theta = \theta^{(0)} + \varepsilon\theta^{(1)} + O(\varepsilon^2)$. The zeroth-order solution $\theta^{(0)}$ is the SS solution at $\omega_0 = 1$ given earlier. At the next order, the solution is $\theta^{(1)} = e^{\alpha t}\left[C_1\cos(\beta t) + C_2\sin(\beta t)\right] + C_3\sin(t + \Phi)$, with constants α, β, C_i, Φ. In particular, $\alpha = -\frac{1+G^2}{(1+2G^2)G} < 0$, which suggests that at large times ($t \to \infty$), the dynamics is dominated by $C_3\sin(t + \Phi)$ and the particle settles into a periodic orbit with time period 2π, which is consistent with the plots in Fig. 2(b) for the smaller values of ε. Likewise, in the TU regime, we performed another perturbation analysis for an almost rigid particle ($G \ll 1$). It is straightforward to show that the leading-order solution for θ recovers the classical Jeffery's orbit for a rigid particle [20]: $\tan(\theta) = \omega_0\tan\left(-\frac{\pi t}{T}\right)$, with period $T = \pi\left(\omega_0 + 1/\omega_0\right)$.

Next, we address in more detail the transition from the TR to the TU regimes aiming to construct a "phase diagram" for the particle motion in the parameter space defined by G and ω_0. Before doing so, it is important to emphasize that the dynamics in this Letter refers to

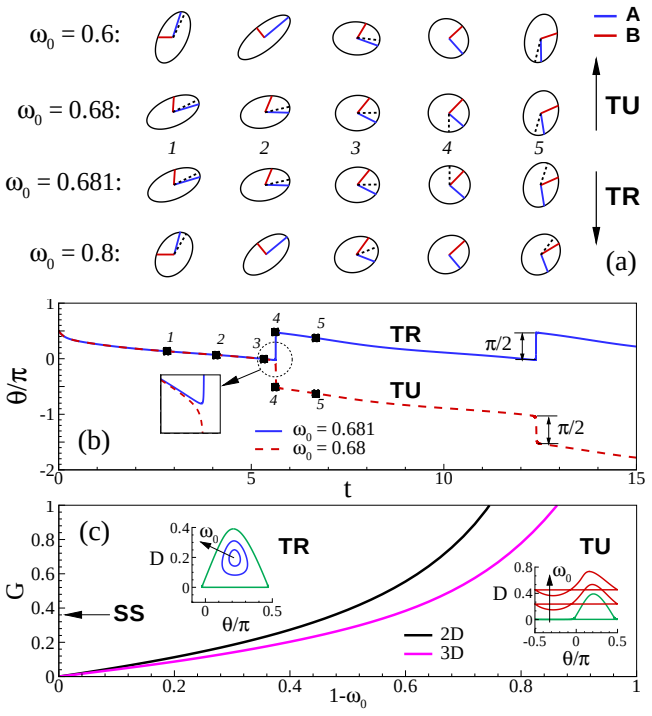

FIG. 3: (a) Snapshots of 2D shape contours at five sequential time instants for $G = 0.2$, where the TR/TU transition happens at $\omega_0^* \sim 0.68$. The blue and red lines represent two material lines initially coinciding with the semi-major and semi-minor axes of the particle, while the dashed black lines represent the "current" semi-major axis. (b) Bifurcation in θ near the TR/TU transition for a 2D particle. (c) Phase diagram for both a 2D and a 3D (initially prolate spheroidal) particles under shear. Insets in (c): Typical $D - \theta$ orbits for a 2D particle in the two regimes at $G = 0.2$, $0.3 \leq \omega_0 \leq 0.9$. The arrows show the direction of decreasing ω_0.

"shape" dynamics (or morphologies) for the soft particles [4]. In fact, the material elements in the particle undergo only one type motion—a continuous TT motion where the material lines going through the particle center spin continuously in the CW direction. However, as a consequence of the competition between the hydrodynamic forces that tend to stretch material line elements instantaneously coinciding with the maximum stretch direction $(+\pi/4)$ and the restoring elastic forces that tend to resist this stretch, the long axis of the particle in its current (or deformed) state is not necessarily always the initial (reference) long axis of the elliptical particle. If, for a given initial particle shape ω_0, the hydrodynamic forces are not sufficiently strong compared to the elastic forces in the particle—tending to preserve its initial shape—the particle will tumble; otherwise, it will tremble (or reach a steady state if the particle is initially circular). More precisely, making use of the fact that an initially straight material line remains straight in a linear deformation field, we can visualize the particle motion by tracking two special material lines initially coinciding with the semi-major (A) and semi-minor (B) axes. From Fig. 3(a), both lines A and B continue to spin in the CW direction. However, in the TU regime, the length of B (l_B) is always shorter than that of A (l_A), while in the TR regime, l_A and l_B exceed each other in an alternating fashion. Correspondingly, the current long axis of the particle (dashed-black line) completes a full rotation in the TU regime, while it swings back and forth in the TR regime. Clearly, the critical condition for the TR/TU transition corresponds to the situation when l_B only reaches l_A without ever exceeding it—the current particle shape then becomes instantaneously circular ($\omega = 1$). The critical behavior of θ is highlighted in Fig. 3(b) by two different time-evolution curves for θ at $G = 0.2$, with $\omega_0 = 0.68$, and 0.681. As can be seen by following the 5 sequential time instants marked with black squares, and corresponding to the same times shown in Fig. 3(a), a bifurcation in θ occurs with a jump of either $-\frac{\pi}{2}$ (TU) or $+\frac{\pi}{2}$ (TR).

Having characterized the TR/TU transition, it is now a simple matter to construct the (2D) phase diagram, which is shown in Fig. 3(c) for arbitrary G and ω_0. Thus, as ω_0 is reduced from 1 with G fixed, the particle motion changes from SS to TR, and in turn to TU, as was seen in Fig. 1. On the other hand, as G is increased for any initially non-circular shape ($\omega_0 < 1$), a transition from TU to TR is observed. In addition, plots are included as insets in Fig. 3(c) of the D versus θ orbits (where $D = \frac{1-\omega}{1+\omega}$ is the deformation parameter). They show that with decreasing ω_0 the orbits become larger in the TR regime tending to a dumbell shape at the transition, and then to a skew "8" shape in the TU regime. The nature of the TR/TU transition near the origin can be clarified using a "mixed" perturbation analysis for a nearly circular ($\omega_0 = 1 - \varepsilon, \varepsilon \ll 1$) and almost rigid ($G \ll 1$) particle, with $G = k\varepsilon$, for some constant k. Interestingly, to the leading order, the variables τ_{11}^p, ω and θ satisfy the relation: $\left[\omega\left(\tau_{11}^p + \frac{1}{G}\right)\right]^2 = \frac{1}{k^2} - 4(\cos 2\theta)^2 \geq 0$. It follows that a solution allowing arbitrary values of θ—and corresponding to a typical TU motion—is possible for $k < \frac{1}{2}$. On the other hand, for $k > \frac{1}{2}$, a (real) solution exists only when θ is restricted to the interval $\left[\frac{1}{2}\arccos\left(\frac{1}{2k}\right), \frac{\pi}{2} - \frac{1}{2}\arccos\left(\frac{1}{2k}\right)\right]$, corresponding to TR motions. Therefore, in the region where both G and ε are small, the condition for the TR/TU transition is simply $G^* = \frac{1-\omega_0}{2}$.

For an initially spheroidal (3D) elastic particle undergoing planar motions in the shear plane, completely analogous results are obtained. In particular, the SS motion for an initially spherical particle is found to be stable, and the same mechanism described above can be used to explain the TR/TU transition for the 3D elastic particles when the projection of the particle onto the shear plane becomes circular. The phase diagram for the case of initially prolate spheroidal particles, with initial aspect ratio ω_0, is also shown in Fig. 3(c), for completeness.

Using the single-particle dynamics, we can calculate the rheological properties of a dilute suspension (concen-

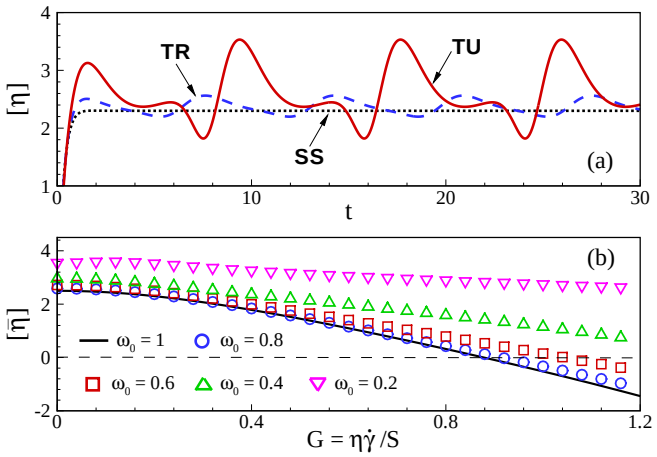

FIG. 4: The intrinsic viscosity $[\eta]$ of a dilute suspension of initially prolate spheroidal, neo-Hookean particles. (a) Time evolution of $[\eta]$ in the three regimes (SS, TR and TU) for $G = 0.2$. The dotted-black, dashed-blue and solid-red lines denote results for $\omega_0 = 1, 0.8$ and 0.5, respectively. (b) Mean values of $[\eta]$, as functions of G, for several values of ω_0.

tration $\phi \ll 1$) of such soft particles [15, 21]. Depending on the initial shape of the prolate spheroidal particles, the rheological response will either tend to a steady state or to a periodic, time-dependent response. Fig. 4(a) shows plots of the intrinsic viscosity $[\eta]$ (see its definition in [21]) for $G = 0.2$ and three different values of ω_0 in the SS (1), TR (0.8) and TU (0.5) regimes. For initially spherical ($\omega_0 = 1$) particles, all particles reach a stable configuration with a shear-thinning effect [15]. (Note that $[\eta]$ becomes negative for large G.) For initially non-spherical particles, we make use of the time average of $[\eta]$ over one period (for a single particle), $[\bar{\eta}]$, as a simple measurement of the mean viscosity of a dilute suspension of uncorrelated particles [9, 20, 22]. As shown in Fig. 4(b), suspensions of deformable particles generally exhibit shear-thinning, although the effect becomes less pronounced with decreasing aspect ratio ω_0. It also shows that, for given $\dot{\gamma}$, $[\bar{\eta}]$ drops with particle stiffness S, although, again, deviations from perfectly spherical shapes tend to weaken the effect. These phenomena may be explained by noting that compared to an initially spherical particle, the unsteady rotation of an initially non-spherical particle generates larger disturbances in the flow, and therefore leads to higher intrinsic viscosity for the suspension.

In conclusion, three different types of motion have been identified for elastic particles in an unbounded shear flow, depending on their initial aspect ratio ω_0 and the stiffness parameter G. They are globally similar to those observed in vesicle motions under shear [5–9], but the phase diagram is simpler, not allowing SS motion for initially non-spherical particles, nor direct transitions from the SS to the TU regime. The results for the rheological properties are also different, since—even for initially non-spherical particles—the intrinsic viscosity can become negative for sufficiently soft particles (large G). It is hoped that the results of this study will help guide future experimental work on the response of soft elastic particles in microscale fluidic environments. A more complete study, including generally ellipsoidal shapes and more complex out-of-plane motions will be presented elsewhere.

We acknowledge the support from the Nano/Bio Interface Center at the University of Pennsylvania through the NSF NSEC DMR-045780 (TG and HHH), and the National Science Foundation under NSF Grant No. CMMI-0969570 (PPC). We also gratefully acknowledge critical reading and comments on the paper by P. E. Arratia.

[1] R. Skalak and P. I. Branemark, Science **9**, 717 (1969).
[2] U. Seifert, Adv. Phys. **46**, 13 (1997).
[3] J. K. Oh, R. Drumright, D. J. Siegwart, and K. Matyjaszewski, Prog. Polym. Sci. **33**, 448 (2008).
[4] M. Kraus, W. Wintz, U. Seifert, and R. Lipowsky, Phys. Rev. Lett. **77**, 3685 (1996).
[5] V. Kantsler and V. Steinberg, Phys. Rev. Lett. **96**, 036001 (2006).
[6] C. Misbah, Phys. Rev. Lett. **96**, 028104 (2006).
[7] V. V. Lebedev, K. S. Turitsyn, and S. S. Vergeles, Phys. Rev. Lett. **99**, 218101 (2007).
[8] H. Noguchi and G. Gompper, Phys. Rev. Lett. **98**, 128103 (2007).
[9] H. Zhao and E. S. G. Shaqfeh, J. Fluid Mech. **674**, 578 (2011).
[10] P. M. Vlahovska, Y. -N. Young, G. Danker, and C. Misbah, J. Fluid Mech. **678**, 221 (2011).
[11] R. Roscoe, J. Fluid Mech. **28**, 273 (1967).
[12] J. D. Goddard and C. Miller, J. Fluid Mech. **28**, 657 (1967).
[13] R. Pal, *Rheology of particulate dispersions and composites*, (CRC Press, 2007).
[14] P. Le Tallec and J. Mouro, Comput. Methods Appl. Mech. Eng. **190**, 3039 (2001).
[15] T. Gao, H. H. Hu, and P. Ponte Castañeda, J. Fluid Mech. (accepted).
[16] J. D. Eshelby, Proc. R. Soc. Lond. A **241**, 376 (1957).
[17] J. R. Willis, Adv. Appl. Mech **21**, 1 (1981).
[18] M. Kailasam and P. Ponte Castañeda, J. Mech. Phys. Solids **46**, 427 (1998)
[19] T. Gao and H. H. Hu, J. Comput. Phys. **228**, 2132 (2009).
[20] G. B. Jeffery, Proc. R. Soc. Lond. A **102**, 161 (1922).
[21] See supplementary material.
[22] G. Danker and C. Misbah, Phys. Rev. Lett. **98**, 088104 (2007).